Combustion and Flame 256 (2023) 112940

Contents lists available at ScienceDirect

Combustion and Flame

journal homepage: www.elsevier.com/locate/combustflame

Extension of the layer particle model for volumetric conversion reactions during char gasification

Thomas Steiner[a,b,*], Kai Schulze[b], Robert Scharler[a], Andrés Anca-Couce[a,c]

[a] Institute of Thermal Engineering, Graz University of Technology, Inffeldgasse 25/B, 8010 Graz, Austria
[b] BEST - Bioenergy and Sustainable Technologies GmbH, Inffeldgasse 21b, 8010 Graz, Austria
[c] Thermal and Fluids Engineering Department, Carlos III University of Madrid, Avda. de la Universidad 30, Madrid, 28911 Leganés, Spain

ARTICLE INFO

Article history:
Received 3 October 2022
Revised 23 June 2023
Accepted 4 July 2023
Available online 14 July 2023

Keywords:
Biomass
Thermochemical conversion
Char conversion
Gasification
Particle model
Effectiveness factor

ABSTRACT

The so-called "layer model" or "interface-based model" is a simplified single particle model, originally developed for shorter computation time during computational fluid dynamics (CFD) simulations. A reactive biomass particle is assumed to consist of successive layers, in which drying, pyrolysis and char conversion occur sequentially. The interfaces between these layers are the reaction fronts. The model has already been validated for drying, pyrolysis and char oxidation. Layer models in the literature have commonly employed surface reactions at the reaction front to describe char conversion. In this work, the suitability of this surface reaction concept is assessed when gasifying biochar. It is shown that a particular layer model, already available, which originally employed surface reactions, was unable to adequately describe the mass loss during gasification of a biochar. In order to overcome this incapability, the model was extended to consider volumetric reactions in the char layer. The influence of intraparticle diffusion was considered through an effectiveness factor. The model is easily adaptable for different gas-solid kinetic rate laws, while still allowing for comparably fast solutions of the model equations. The extended model was validated using theoretical calculations and experimental measurements from literature. It was demonstrated that intraparticle diffusion can significantly slow down the biochar gasification process. A general guideline for when to employ volumetric reactions, rather than surface reactions, and when to consider intraparticle diffusion is provided based on the Thiele modulus as the criterion.

1. Introduction

The thermochemical conversion of biomass typically consists of the following consecutive steps: drying, pyrolysis and char conversion (oxidation and gasification). Depending on the application, some of these steps may not be relevant [1]. During thermochemical conversion, chemical reactions and transport processes at the particle level can both be important (and also limiting), which calls for suitable models at these scales. Fast-solving and oftentimes simplified models are required for computational fluid dynamics (CFD) simulations with a high number of particles. Haberle et al. [2] have given an overview of the state-of-the-art particle models for biomass conversion. They can be categorized according to two classes: Mesh-based (or volumetric) models and interface-based (or layer) models. Note that throughout this work "layer model" in lower case letters refers to interface-based models in a general sense. "Layer Model" in capital letters refers to the specific layer model of Mehrabian et al. [3], which is employed and adapted in this work.

Figure 1 summarizes the differences between volumetric and layer models. It also compares the number of balance equations to be solved for temperatures T, concentrations c_A and partial densities ρ_k^e. On the one hand, volumetric models use a (typically 1D) spatial discretization of the particle with a sufficient resolution and solve the conservation equations. This approach is more comprehensive, but can be numerically costly, depending on the number of control volumes and the number of equations to be solved. In the literature, several volumetric models are available which can predict the processes during thermochemical conversion at particle level with good accuracy while employing a high number of equations (see e.g., [4–8]). On the other hand, layer models (e.g., [3,9–11]) treat particles as discrete volumes which are coupled to each other through interfaces, also called boundaries. These interfaces typically represent the reaction fronts. The volumes (the so-called

* Corresponding author.
E-mail address: thomas.steiner@best-research.eu (T. Steiner).

https://doi.org/10.1016/j.combustflame.2023.112940

Nomenclature

A	(surface) area in m^2
Bi_M	mass transfer Biot number
c	concentration in $kmol \cdot m^{-3}$
c_P	specific heat capacity in $J \cdot kg^{-1} \cdot K^{-1}$
d	diameter in m
D_e	effective diffusivity in $m^2 \cdot s^{-1}$
E_A	activation energy in $kJ \cdot mol^{-1}$
f_{shape}	shape factor
$F(X)$	concentration of active solid sites
h	specific enthalpy in $J \cdot kg^{-1}$
k	(surface) reaction rate constant in $m \cdot s^{-1}$ or other units as stated in text
k_c	reaction rate constant in $kmol^{1-n} \cdot s^{-1} \cdot m^{3(n-1)}$
K	reaction rate constant in $atm^{-n} \cdot s^{-1}$
K_c	reaction rate constant in $m^{3n} \cdot kmol^{-n} \cdot s^{-1}$
K_0	pre-exponential factor in $atm^{-n} \cdot s^{-1}$
$K_{c,0}$	pre-exponential factor in $m^{3n} \cdot kmol^{-n} \cdot s^{-1}$
L	length in m
m	mass in kg
$\dot{m}$	mass flow in $kg \cdot s^{-1}$
M	molar mass in $kg \cdot kmol^{-1}$
n	order of reaction
N	number (of species, equations, ...)
$\dot{N}$	consumption/flow rate in $kmol \cdot s^{-1}$
p	partial pressure in atm
r	radius, spatial coordinate in m
$\dot{r}$	volumetric rate of reaction in $kmol \cdot m^{-3} \cdot s$
R	radius of particle (at ash layer surface) in m
R	normalized rate of reaction in s^{-1}
$\dot{R}$	rate of reaction in $kmol \cdot s^{-1}$ or $kg \cdot s^{-1}$
R_{gas}	universal gas constant in $J \cdot kmol^{-1} \cdot K^{-1}$
S	specific surface area in m^{-1}
T	temperature in K
t	time in s
V	volume in m^3
x	molar fraction
X	conversion
Δx_0	characteristic conduction length from left layer boundary to layer center in m
Δx_1	characteristic conduction length from layer center to right layer boundary in m

Greek Symbols

β	mass transfer coefficient in $m \cdot s^{-1}$
δ_{err}	estimated relative error
ε	porosity
η	effectiveness factor
γ	shape factor/exponent
λ	thermal conductivity in $W \cdot m^{-1} \cdot K^{-1}$
Λ	characteristic length in m
ν	stoichiometric coefficient
Φ	Thiele modulus
ρ	density in $kg \cdot m^{-3}$

Sub-/Superscripts

0	initial or pre-exponential
A	gaseous component
act	actual, observed
ash	ash layer
B_i	boundary
C	char
CV	control volume
diff	intraparticle-diffusion-limited
e	effective
ext	external
i	index
int	internal
k	component index
L_i	layer
p	particle
R	at ash layer surface (particle surface)
S	at char layer surface
tot	total
∞	at bulk conditions, in equilibrium or final

layers) represent the relevant states in thermochemical conversion (wet wood, dry wood, char, sometimes residual ash). A significantly reduced number of volumes is thus required compared to mesh-based methods. Usually there are also major simplifications regarding the transport of gaseous species within the porous particle, leading to a strongly reduced set of transport equations to be solved. Thunman et al. [9] provided the concept in the context of biomass conversion, which has been taken as a basis for the Layer Model used in this work, as originally published by Mehrabian et al. [3]. It has shown to be computationally efficient, coupling the single particle model to CFD simulations [12] with a reasonable calculation time.

In the literature, there are several instances of layer models validated with experimental data and showing good results for pyrolysis and combustion of dry and wet biomass particles [3,9–11,13]. This can usually be modeled conveniently using surface reactions at the reaction front, because at high reaction rates the incoming oxygen is rapidly consumed at the interface. Recently, Li et al. [14] published their modification of the layer model by Thunman et al. [9], increasing the spatial resolution through introduction of a finite-volume mesh. Due to their focus on combustion, however, the gasification reactions have unfortunately been entirely neglected. He and Behrendt [15] combined a volumetric model approach with a layer model approach using a similar reasoning to that employed in this work. This provides the possibility to resolve broader reaction regions with the volumetric model and the simplified handling of narrow reaction regions at reaction fronts. Gasification, however, is not considered.

Despite its validation for pyrolysis and combustion and despite the ongoing endeavors to improve the layer model concept, to the best of our knowledge, the layer model has yet to be validated for gasification. In Mehrabian et al. [3], the gasification reactions were modeled via surface kinetics given by [16]. These kinetics were also used for example by Thunman et al. [9], Johansson et al. [17] and Gómez et al. [11]. Typically, the gasification reactions have been included in layer models (which mostly focus on pyrolysis and/or combustion) without specific validation. In contrast to the oxidation reactions, the gasification reactions show much lower intrinsic reaction rates at typical temperatures (923 – 1273 K) [18]. Gaseous reactants might not be rapidly consumed at the external surface, but can instead diffuse inside the porous network of the particle. Then the conversion does not only take place at the outer boundary of the char layer but also within the layer itself. As will be shown in Section 3, the description of char gasification as a simple surface reaction at the reaction front is not applicable for the general case.

In practice, biomass gasification is a relevant process for combined heat and power (CHP), second generation biofuels and biorefinery concepts [19]. In the context of general char conversion (i.e. in conjunction with oxidation) it usually plays a secondary role due to the high reaction rate of char oxidation. There are various appli-

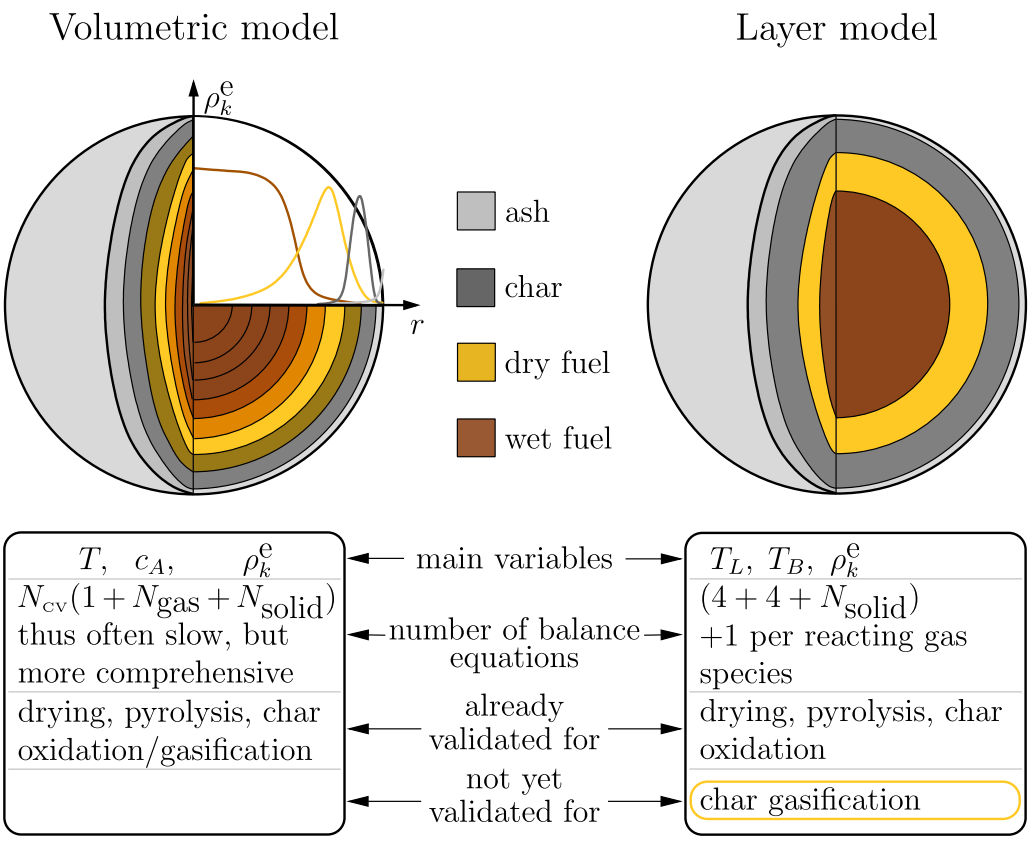

Fig. 1. A biomass particle described through the volumetric model and layer model. (CV…control volume, *L*…layer, *B*…boundary).

cations, however, in which gasification is of high relevance. This is the case for example when gasification is the main process of interest [20], during slow oxidation and when parts of the system act as a dedicated gasification zone [21]. Moreover, biomass can be used as a fuel in chemical looping combustion (CLC) [22,23] or gasification (CLG) processes [24], in which in-situ gasification is typically the limiting step for overall conversion. In future, biomass gasification might also prove to be useful for chemical looping hydrogen (CLH) production [25]. To sum up, reliable models for this conversion process are required due to the high relevance of biomass gasification.

The aims of this work are to (a) assess the Layer Model [3] for describing char gasification and (b) to improve this type of model to predict char gasification with good accuracy for all relevant cases. For this purpose, a novel volumetric gas-solid reaction model for char conversion is suggested, as explained in Section 2, instead of the currently employed surface kinetics at the reaction front. The flexible volumetric extension for the Layer Model is able to consider char conversion reactions in the whole char layer and estimate the effect of intraparticle diffusion through an effectiveness factor approach. This allows for an approximation of the internal gas concentration field without actually solving the species conservation equations for every time step, thus saving computation time. The approach presented is first compared to theoretical solutions for simple cases. The volumetric kinetics and experimental measurements by Van de steene et al. [8] and Mermoud et al. [7] are then used to showcase the suitability of the computationally fast, extended Layer Model for biochar gasification. It is shown that the original surface-kinetics-model, despite its common application in the literature [3,9,11,17], is unable to predict the experimental data. This is primarily due to the scaling of reaction rates with external char layer surface area instead of char layer volume. A general guideline for when to apply volumetric reactions versus surface reactions based on the Thiele modulus Φ is established. The necessity of intraparticle diffusion modeling is also assessed. Finally, the advantages and possible shortcoming of the novel, extended Layer Model formulation are discussed.

2. Char conversion modeling

2.1. Layer model

Before going into the derivation of the novel modeling approach, the Layer Model concepts essential to this work shall be briefly outlined (for details see [3]). In biomass conversion, the Layer Model describes a biomass particle as four layered volumes. These interconnected, integral layers can exchange energy and mass. Between two neighboring layers there is always an interface (a boundary), which separates them from each other. This boundary also constitutes the external surface area of the inner layer. Each layer represents an individual sub-step in biomass conversion, as shown in Fig. 1. In the beginning, an entire wet biomass particle is constituted by the first and central layer. It consists of (dry) biomass and water. The other, initially empty, layers are subsequently filled and depleted during the conversion process. The water is evaporated during drying and the drying front moves towards the center. The resulting dry biomass constitutes the second layer. Through pyrolysis the volatiles are released from the particle and the residual char, which consists of carbon and ash, makes up the third layer. The fourth, last and outermost layer consists only of ash. It is filled when the carbon from the third layer is converted through gasification and/or oxidation. In practice, all four layers can be active at the same time, since all the sub-steps of the conversion process can take place in parallel.

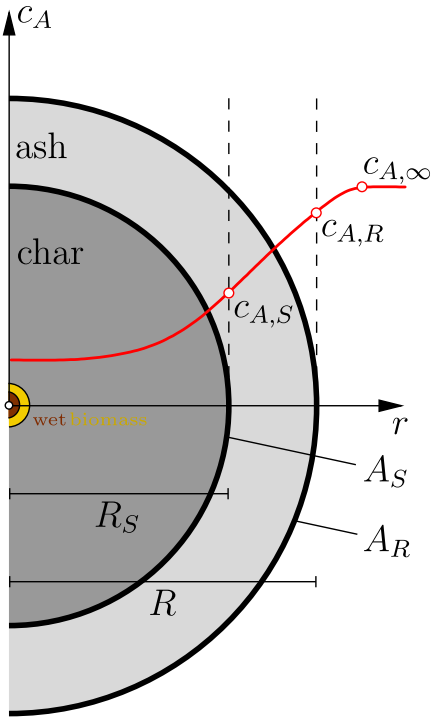

Fig. 2. Porous biomass particle with concentration of gaseous species A in the bulk $c_{A,\infty}$, at the ash-layer-surface $c_{A,R}$ and at the char-layer-surface $c_{A,S}$.

The general, mathematical framework of layer models has been presented in the literature many times (e.g., [3,9,10,13]). This work is based on the Layer Model by Mehrabian et al. [3], which is briefly summarized in the Supplementary Material. Since this work focuses on char conversion, the modeling of drying and pyrolysis is not discussed. As stated in Section 1, layer models have already been validated for these processes. Thus, only the equations relevant to char conversion are discussed.

In the original Layer Model, char conversion only takes place in the char layer boundary (i.e. the infintely thin, external surface of the char layer). The char is assumed to consist of carbon and ash, with ash being an inert component. A total of four char conversion reactions are considered:

$$\nu_C\,C + O_2 \longrightarrow 2(\nu_C - 1)\,CO + (2 - \nu_C)\,CO_2 \quad \text{(R1)}$$
$$C + CO_2 \longrightarrow 2\,CO \quad \text{(R2)}$$
$$C + H_2O \longrightarrow CO + H_2 \quad \text{(R3)}$$
$$C + 2\,H_2 \longrightarrow CH_4 \quad \text{(R4)}$$

For single particle oxidation, where reaction (R1) is the most important one, the Layer Model is already validated [3]. The reactions (R2) and (R3) are of specific interest for gasification, while reaction (R4) is usually much slower.

Figure 2 shows an exemplary biomass particle with the assumed geometric specifications and concentrations of gaseous reactant A. The 1D transient reaction-diffusion equation for a gaseous species A within a porous biomass particle layer can be written as

$$\varepsilon \frac{\partial c_A}{\partial t} = \frac{1}{r^\gamma}\frac{\partial}{\partial r}\left(r^\gamma D_{e,A}\frac{\partial c_A}{\partial r}\right) + \dot{r}_A \tag{1}$$

where γ can take values of 0, 1 or 2, depending on the geometric shape of the particle (slab, cylinder or sphere, respectively). Diffusional fluxes are modeled using Fickian diffusion, which is a simplification in view of the general case of multicomponent mass transfer [26]. During the char conversion process, an inert, porous ash layer is forming on the outside of the particle. Gaseous components have to be transported through this inert layer to reach the reactive char layer for gasification and oxidation. With the particle radius R and the radius at the char layer surface R_S, following the work of Wen [27], the conservation Eq. (1) within the ash layer can be simplified to

$$0 = D_{e,A}^{ash}\frac{1}{r^\gamma}\frac{d}{dr}\left(r^\gamma\frac{dc_A}{dr}\right) \qquad (R_S \le r \le R). \tag{2}$$

The assumptions which lead from Eq. (1) to (2) are

- pseudo-steady-state, which is a reasonable approximation for many gas-solid reactions [27],
- no reactions within the inert, porous ash layer,
- radially-independent effective diffusion coefficient $D_{e,A}^{ash}$.

There are three possibly limiting mechanisms during char conversion in the Layer Model: External mass transfer, internal mass transfer through the ash layer and chemical reactions. At pseudo-steady state, their transport/consumption rates $\dot{N}_A$ of gaseous reactant A are equal.

$$-\dot{N}_A = A_R\,\beta\,(c_{A,\infty} - c_{A,R}) \tag{3}$$

$$-\dot{N}_A = A(r)\,D_{e,A}^{ash}\frac{dc_A}{dr} \qquad (R_S \le r \le R) \tag{4}$$

$$-\dot{N}_A = -\dot{R}_A \tag{5}$$

A is the surface area, c is the concentration, β is the mass transfer coefficient. The index R signifies the particle (= ash layer) surface, index S signifies the char layer surface and index ∞ signifies bulk conditions.

In the following part, two methods for closing the reactive expression $\dot{R}_A$ in Eq. (5) are presented. The first method - using surface reactions - was employed in the original Layer Model of Mehrabian et al. [3]. The second method - using volumetric reactions - is new and leads to an "Extended Layer Model" with significant improvements for general char conversion modeling.

2.2. Original model - surface reactions

In the original Layer Model, char conversion only takes place at the char layer boundary (i.e. the infintely thin, external surface of the char layer). The molar conversion rates for reactions (R1)–(R4) at the particle scale are proportional to the *external* char surface area A_S. They are thus labeled "surface reactions" in this work. The model uses first order kinetics of the form

$$-\dot{R}_A = -\frac{\nu_A}{\nu_C}\dot{R}_C = A_S\,k_A\,c_A \tag{6}$$

where A_S is the surface area of the char layer boundary, c is the concentration, ν are the stoichiometric coefficients and the subscripts C and A indicate char and the respective gaseous reactant for reactions (R1)–(R4), respectively. The expressions for k_A are presented in Table 1.

Table 1
Intrinsic kinetic parameters [9,16] of char conversion surface reactions as used by Mehrabian et al. [3].

Reactant A	k_A / m · s^{-1} (with T in K)
O_2	$1.715 \cdot T \exp\left(\frac{-9000}{T}\right)$
H_2O/CO_2	$3.42 \cdot T \exp\left(\frac{-15600}{T}\right)$
H_2	$3.42 \cdot 10^{-3} \cdot T \exp\left(\frac{-15600}{T}\right)$

Note that in the case of only surface reactions, in Fig. 2 the concentration c_A is zero for $r < R_S$. Combining Eqs. (3)–(5) for surface reactions gives the following boundary conditions

$$A_R\,\beta\,(c_{A,\infty} - c_{A,R}) = A(r)\,D_{e,A}^{ash}\frac{dc_A}{dr} = A_S\,k_A\,c_{A,S}. \tag{7}$$

The detailed derivation is presented in the Supplementary Material. The final, total char conversion rate is the sum of the conversion rates from reactions (R1)-(R4)

$$-\dot{R}_C = \sum_{R1-R4} \frac{\frac{\nu_C}{\nu_A} M_C c_{A,\infty}}{\frac{1}{k_A A_S} + \frac{1}{\beta A_R} + \frac{1}{D^{ash}_{e,A}} \int_{R_S}^{R} \frac{dr}{A(r)}} \tag{8}$$

where M_C is the molar mass of carbon.

2.3. Extended model - volumetric char conversion reactions

In the new, extended Layer Model, char conversion does not necessarily take place only at the char layer boundary. Instead, it can take place in the entirety of the char layer. The molar conversion rates for reactions (R1)-(R4) at the particle scale are proportional to the char layer volume V_C (or mass). They are thus labeled "volumetric reactions" in this work. Two volumetric rate laws are used in this work, as detailed in Section 2.4. In general, they take the form

$$-\dot{R}_A = -\dot{r}_A V_C. \tag{9}$$

Combining Eqs. (3)–(5) for volumetric reactions gives the following boundary conditions

$$A_R\, \beta (c_{A,\infty} - c_{A,R}) = A(r)\, D^{ash}_{e,A} \frac{dc_A}{dr} = -\dot{r}^{act}_A V_C. \tag{10}$$

The actual (or observed) volumetric reaction rate $\dot{r}^{act}_A$ is linked to the volumetric reaction rate at char-layer-surface-conditions $\dot{r}_{A,S}$ through the effectiveness factor η.

$$\eta(\Phi) = \eta_{int}(\Phi) = \frac{\dot{r}^{act}_A}{\dot{r}_{A,S}} \tag{11}$$

It is a well-known modeling approach for heterogeneous catalysis [28] and can also be applied for char gasification [29–32]. Thus, the actual reaction rate $\dot{r}^{act}_A$ can be computed without solving the transport equations of all gaseous species, which would drastically increase the computational effort. Following the nomenclature in [32], this effectiveness factor is also referred to as the internal effectiveness factor η_{int}. If not stated differently, the term effectiveness factor η without further specification always refers to this internal effectiveness factor η_{int} throughout this work.

The effectiveness factor $\eta(\Phi)$ depends on the dimensionless Thiele modulus Φ, which is given for example in [28] for an irreversible reaction of order n. Accordingly, we use

$$\Phi = \Lambda \cdot \sqrt{\frac{(n+1) k_c c^{n-1}_{A,S} F(X)}{2 D^{C}_{e,A}}} \tag{12}$$

which additionally considers the current, overall conversion state through $F(X)$, as explained in Section 2.4. The volume-to-surface-area ratio of the char layer is chosen as the characteristic length Λ [33]. Note that $D^{C}_{e,A}$ denotes the effective diffusion coefficient in the porous char layer, as opposed to $D^{ash}_{e,A}$ in the porous, inert ash layer. According to Mehrabian et al. [3], the effective diffusion coefficients are calculated from Knudsen diffusivities $D_{A,Kn}$ and binary molecular diffusivities D_{A-N_2} in nitrogen. Even though the char and ash layers have different properties, for the cases presented in this work, the same binary molecular and Knudsen diffusion coefficients are taken for both of them. Hence, the effective diffusion coefficients only differ through the char and ash layer porosities.

$$D^{C}_{e,A} = \left(\frac{\varepsilon_C}{\varepsilon_{ash}}\right)^2 D^{ash}_{e,A} = \left(\frac{\varepsilon_C}{\varepsilon_{ash}}\right)^2 \varepsilon^2_{ash} \left(\frac{1}{D_{A-N_2}} + \frac{1}{D_{A,Kn}}\right)^{-1} \tag{13}$$

Different correlations for obtaining the effectiveness factor η as a function of the Thiele modulus Φ can be found in the literature.

Table 2
General, kinetics-related equations and kinetic models by Van de steene et al. [8] and Mermoud et al. [7].

General equations
$X = \frac{m_{C,0} - m_C}{m_{C,0}}$
$-R_C = -\frac{1}{m_C}\frac{dm_C}{dt} = \frac{1}{1-X}\frac{dX}{dt}$
$\eta_{int} = \frac{1}{\Phi}\left(\frac{1}{\tanh(3\Phi)} - \frac{1}{3\Phi}\right)$
$\Lambda = (V/A)_C$
Kinetic models
Van de steene et al. [8]
$-R_C = K \cdot p^n_A \cdot F(X) = K_c \cdot c^n_A \cdot F(X)$
$K = K_0 \exp\left(\frac{-E_A}{R_{gas} T}\right)$ or $K_c = K_{c,0} \exp\left(\frac{-E_A}{R_{gas} T}\right)$
$-\dot{r}_C = k_c \cdot c^n_A \cdot F(X)$
$k_c = c_{C,0} K \left(R_{gas} T\right)^n$
$\Phi = \Lambda \cdot \sqrt{\frac{(n+1) k_c c^{n-1}_{A,S} F(X)}{2 D^{C}_{e,A}}}$
Mermoud et al. [7]
$-\dot{r}_C = \frac{k_1 p_{H_2O} + k_4 p_{H_2} p_{H_2O} + k_5 p^2_{H_2O}}{1 + k_2 p_{H_2} + k_3 p_{H_2O}} c_C S_{int}$
$S_{int} = (2.75 \cdot 10^8\ m^{-1})/(1-X)$
$\Phi = \frac{\Lambda \cdot \dot{r}_{A,S}}{\sqrt{2 D^{C}_{e,A} \int_0^{c_{A,S}} \dot{r}(c)\, dc}}$

Several of these [28,34–37] were tested for the cases reported in this study. They all yielded similar results, when the correct respective formulation of the Thiele modulus Φ was used. For the numerical results in this work, the classic analytical solution for first order reactions in spheres is used [37].

$$\eta(\Phi) = \eta_{int}(\Phi) = \frac{1}{\Phi}\left(\frac{1}{\tanh(3\Phi)} - \frac{1}{3\Phi}\right) \tag{14}$$

It is known that the differences between η-solutions for spheres, cylinders and slabs are rather small, if the Thiele modulus Φ is properly scaled [33]. Therefore, the volume-to-surface-area ratio is used as characteristic length Λ, as given in Eq. (12). Similarly, the proper definition of the Thiele modulus Φ allows for using Eq. (14) for reaction orders different than one [38].

2.4. Volumetric kinetics

Table 2 summarizes the kinetics-related equations used in the extended Layer Model. Complete reactive char consumption is assumed for the conversion X and the reactivity R_C [8]. Note that in contrast to [8] the reactivity R_C, the integral reaction rates $\dot{R}_C$ and the volume-related reaction rates $\dot{r}_C$ are defined with a negative sign, in order to signalize consumption.

Van de steene et al. [8] reported their kinetics (see Table 3) and experimental measurements for char gasification with H_2O and CO_2 as well as char oxidation. Their original kinetics use the partial pressure p_A of a respective component A as a measure of concentration. Thus, to match their kinetic expression with the one used

Table 3
Intrinsic kinetic parameters of char gasification reactions by Van de steene et al. [8].

Reactant A	K_0 / atm^{-n} · s^{-1}	E_A / kJ · mol^{-1}	n	$F(X)$
H_2O	$35.5 \cdot 10^4$	170.0	0.8	F_{H_2O}
CO_2	$120 \cdot 10^6$	245.0	0.7	F_{CO_2}
$F_{H_2O} = 64.16X^5 - 129.72X^4 + 94.35X^3 - 29.39X^2 + 4.51X + 0.22$				
$F_{CO_2} = 90.90X^5 - 187.23X^4 + 135.12X^3 - 40.59X^2 + 5.55X + 0.65$				

Table 4
Intrisic kinetic parameters of char steam gasification reaction by Mermoud et al. [7], units are adapted for consistency reasons within this work.

Reaction rate constant	Units
$k_1 = 2.09 \cdot 10^{-4} \exp\left(-158.6/(R_{gas}T)\right)$	$m \cdot s^{-1} atm^{-1}$
$k_2 = 1.16 \cdot 10^{-5}$	atm^{-1}
$k_3 = 9.69 \cdot 10^{2} \exp\left(-50.32/(R_{gas}T)\right)$	atm^{-1}
$k_4 = 7.84 \cdot 10^{-7} \exp\left(-95.1/(R_{gas}T)\right)$	$m \cdot s^{-1} atm^{-2}$
$k_5 = 6.38 \cdot 10^{-16}$	$m \cdot s^{-1} atm^{-2}$
R_{gas} in $kJ\,mol^{-1}K^{-1}$, T in K	

in this work, the volumetric reaction rate is adapted to employ the concentration c_A according to Gómez-Barea et al. [32].

Mermoud et al. [7] provided a Langmuir-Hinshelwood rate equation [39] for steam gasification. The kinetic parameters are given in Table 4. Given their more complicated rate law, the more general formulation of the Thiele modulus [38] is applied. Finally, note that the Langmuir-Hinshelwood formulation models the sorption and chemical reaction at the total solid surface area (also internal, porous surface area), not only the external char layer surface area as in the original Layer Model [3]. The internal surface area per volume depends on the char conversion state only and not on the actual particle geometry. Thus, it is labeled as volumetric rate law in this work, because the char conversion rate scales with available char mass instead of external char layer surface area.

2.5. Solution strategy for extended model

Through the introduction of the effectiveness factor η and with volumetric rate laws available, the boundary condition in Eq. (10) can be rewritten as

$$A_R\,\beta\,c_{A,\infty} = A_R\,\beta\,c_{A,R} - V_C\,\eta_{\text{int}}(\Phi(c_{A,S}))\,\dot{r}_{A,S}(c_{A,S}). \tag{15}$$

Both the effectiveness factor $\eta_{\text{int}}(\Phi) = \eta_{\text{int}}(\Phi(c_{A,S}))$ and the rate of reaction at the char layer surface conditions $\dot{r}_{A,S} = \dot{r}_{A,S}(c_{A,S})$ are functions of the yet unknown and desired gas concentration $c_{A,S}$ at the char layer surface. The concentration $c_{A,R}$ at the particle surface is linked to the concentration $c_{A,S}$ at the char layer surface through the solution of Eq. (2). After substraction and by replacing the remaining constant of integration through the boundary condition in Eq. (10), the following expression is obtained.

$$\frac{c_{A,R} - c_{A,S}}{c_{A,\infty} - c_{A,R}} = \frac{\beta R}{D^{\text{ash}}_{\text{e},A}} f_{\text{shape}} \tag{16}$$

Here, the dimensionless group $\beta R/D^{\text{ash}}_{\text{e},A}$ is just the mass transfer Biot number Bi_{M} using the particle radius R as characteristic length. The shape factor f_{shape} is determined by the geometric shape of the particle.

$$\text{slab}: \quad (\gamma = 0) \quad f_{\text{shape}} = 1 - \frac{R_S}{R}$$
$$\text{cylinder}: \quad (\gamma = 1) \quad f_{\text{shape}} = \ln\left(\frac{R}{R_S}\right)$$
$$\text{sphere}: \quad (\gamma = 2) \quad f_{\text{shape}} = \frac{R}{R_S} - 1$$

The lower and upper limits for the concentration $c_{A,R}$ at the ash layer surface are obtained either for vanishing concentrations of A at the char layer surface or at infinitely fast external mass transfer, respectively.

$$c_{A,\infty}\frac{\frac{\beta R}{D^{\text{ash}}_{\text{e},A}} f_{\text{shape}}}{1 + \frac{\beta R}{D^{\text{ash}}_{\text{e},A}} f_{\text{shape}}} \le c_{A,R} \le c_{A,\infty} \tag{17}$$

Combining Eqs. (15) and (16), $c_{A,S}$ can be determined. The type of solution procedure required depends on a few factors. In the simplest case, the effects of intraparticle diffusion can be neglected, leading to $\eta_{\text{int}} = 1$. The non-linearity of the problem then only depends on the mathematical form of $\dot{r}_{A,S}$. For simple rate laws (like first order reactions), an analytical solution for $c_{A,S}$ can be achieved. In the more general case and especially for reaction orders different from one, the problem will be non-linear. It is worth mentioning that, in principle, any rate law formulation can be used for $\dot{r}_{A,S}$. In this work, both rate laws from Table 2 are employed, together with the according Thiele modulus Φ formulations. Equation (15) can be solved using typical methods for non-linear equations with one variable. For this work, Newton's method is used. It is combined with a bisection method if the iteration for $c_{A,S}$ overshoots its physically meaningful boundaries. For all the cases presented here this solution procedure has proven to be fast and reliable, typically leading to convergence within only a few iterations. With $c_{A,S}$ available, the actual reaction rate, the mass loss and the energy equation can readily be updated, as in the original model.

3. Results and discussion

The novel extended Layer Model is validated against theoretical solutions and experimental measurements in Section 3.1. Following this, the improvements achieved by the novel modeling approach are highlighted in Section 3.2. Part of the validation data are used to show that the original Layer Model employing surface reactions is inappropriate for these cases. A general guideline for employing volumetric reactions versus surface reactions for char gasification is established. The importance of intraparticle diffusion modeling is assessed. This leads into a concluding discussion of the model characteristics in Section 3.3.

3.1. Extended model validation

3.1.1. Theoretical validation for different Thiele moduli, Biot numbers and reaction orders

Noorman et al. [40] tested their particle model functionality using the well-known analytical solution for the effectiveness factor η with first order reactions. Despite their work dealing with chemical looping applications and not specifically biomass conversion, the volumetric reaction model for the Layer Model can be tested in a similar fashion. At any given (mass transfer) Biot number, here defined with the radius R,

$$Bi_{\text{M}} = \frac{\beta R}{D^{C}_{e,A}} \tag{18}$$

the overall effectiveness factor η_{tot} can be plotted versus the Thiele modulus Φ and compared to the analytical solution given in [40]. According to Gómez-Barea et al. [32], the overall effectiveness factor η_{tot} can be obtained as the product of the internal effectiveness factor η_{int} and the external effectiveness factor η_{ext}.

$$\eta_{\text{tot}} = \eta_{\text{int}} \cdot \eta_{\text{ext}} = \frac{\dot{r}^{\text{act}}_{A}}{\dot{r}_{A,S}} \cdot \frac{\dot{r}_{A,S}}{\dot{r}_{A,\infty}} = \frac{\dot{r}^{\text{act}}_{A}}{\dot{r}_{A,\infty}} \tag{19}$$

As given in Eq. (19), the internal effectiveness factor η_{int} compares the observed, actual reaction rate $\dot{r}^{\text{act}}_{A}$ to the reaction rate $\dot{r}_{A,S}$ at char layer surface conditions. It considers internal mass transfer limitations through pore diffusion. Furthermore, the external effectiveness factor η_{ext} compares this reaction rate $\dot{r}_{A,S}$ at the char layer surface to the superficial reaction rate $\dot{r}_{A,\infty}$ under bulk conditions. It considers the impact of external mass transfer; here it also contains the effect of the inert ash layer on the rate of reaction within the char layer.

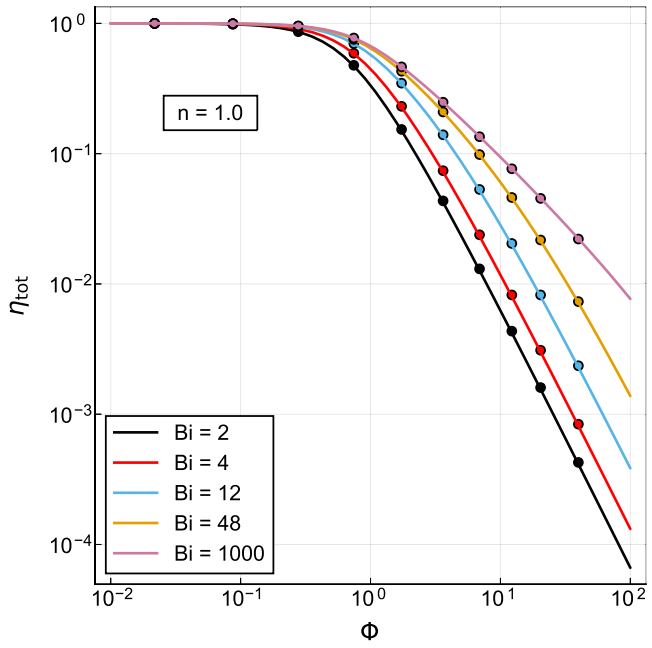

Fig. 3. Extended Layer Model prediction of overall effectiveness factor for a first order volumetric reaction in the char layer for different mass transfer Biot numbers. Solid line depicts the analytical solution, dots are simulation results.

The proposed volumetric extension for the Layer Model uses correlations $\eta(\Phi) = \eta_{int}(\Phi)$ obtained from either analytical solutions [28] or from matching methods [35], as shown in Section 2. Thus, the internal effectivess factor η_{int} is expected to yield reasonable values in any case. However, the effect of external mass transfer and thus η_{ext} on η_{tot} can be analyzed.

For different mass transfer Biot numbers Bi_M, assuming a first order reaction and a char particle without ash layer, the computed overall effectiveness factor η_{tot} is compared to the analytical solution [40] for a spherical particle in Fig. 3. Since only dummy kinetics are required here, those for CO_2 gasification from Table 3 are arbitrarily chosen, assuming $n = 1$. The partial pressure p_{CO_2} is 0.35 atm, the conversion X is 0.25 and the temperature T is varied between 1000 K and 1950 K to obtain different Thiele moduli Φ.

The model is able to reproduce the proper values of the overall effectiveness factor for any of the given Biot numbers. This means that the external mass transfer is suitably described by the model for this simple benchmarking case.

In the Supplementary Material, also different reaction orders n than first order are tested. As expected according to the literature [38], the basic (first order) analytical solutions can be applied with acceptable deviations, given proper scaling of the Thiele modulus Φ.

3.1.2. Validation with char gasification experiments

In order to benchmark the performance of the Layer Model extension, single particle simulations are performed for various experimental cases from the literature. This work employs the experimental measurements as well as intrinsic reaction kinetics for char gasification with H_2O and CO_2 proposed by Van de steene et al. [8] and Mermoud et al. [7]. The volumetric rate expressions are given in Table 2, the respective parameters are summarized in Tables 3 and 4.

The substance property data used during the gasification calculations are given in Table 5. Since their values differ slightly between the experiments, representative values for the effective char density $\rho_C^e = 500\,kg{\cdot}m^{-3}$ and char porosity $\varepsilon_C = 0.75$ are chosen. The influence of the effective ash density ρ_{ash}^e on the mass loss curves was tested for values as low as 50 $kg{\cdot}m^{-3}$ and turned out to be rather small. Diffusion coefficients are obtained as described in [3]. Mass transfer coefficients β are calculated from the Ranz-Marshall-correlation taken from Bird et al. [41] for spherical particles and from the Churchill-Bernstein-correlation [42] for cylindrical particles. Bulk gas properties such as the specific heat capacity c_P, thermal conductivity λ and dynamic viscosity μ are those of nitrogen at the respective bulk temperature taken and, if needed, interpolated from [43]. Drying and pyrolysis are not considered in the simulations. The boundary conditions and particle sizes are those reported by Van de steene et al. [8] and Mermoud et al. [7], respectively. Note that for the cases by Mermoud et al. the given particle diameters (10 mm, 20 mm, 30 mm) are related to initial biomass instead of char. The authors also provide the initial char particle diameters (7.05 mm, 14.07 mm, 20.87 mm), which are taken as initial conditions.

Table 5
Physical property data used for gasification modeling.

Property	Values Used	Units	Reference
$(c_P)_C$	$420 + 2.09T - 6.85 \cdot 10^{-4}T^2$	$J \cdot kg^{-1} \cdot K^{-1}$	[3],*
$(c_P)_{ash}$	$420 + 2.09T - 6.85 \cdot 10^{-4}T^2$	$J \cdot kg^{-1} \cdot K^{-1}$	[3],*
λ_C	0.071	$W \cdot m^{-1} \cdot K^{-1}$	[3],*
λ_{ash}	1.2	$W \cdot m^{-1} \cdot K^{-1}$	[3],*
ρ_C^e	500	$kg \cdot m^{-3}$	[7,8]
ρ_{ash}^e	300	$kg \cdot m^{-3}$	[3]
ε_C	0.75		[7]
ε_{ash}	0.9		[3]
ash content	0.014	$kg \cdot kg_{d.b.}^{-1}$	[8]

* The heat balance equations are provided in the Supplementary Material.

In order to solve the model equations over time, an explicit, fifth order Runge-Kutta-Cash-Karp [44] scheme is applied as in Mehrabian et al [3]. This is especially useful for changing conditions during coupled simulations in a CFD solver like ANSYS Fluent. For the simulations reported in this work, the computation time needed to solve the model equations in C typically ranged from 10 to 30 s on a 4.2 GHz Intel Core i7 processor, with a maximum allowed time step of 0.1 s and simulated times between $3 \cdot 10^3$ s and 10^4 s. The actual time steps usually ranged, except for small initial and final time steps, from 0.01 s to 0.1 s.

Van de steene et al. [8] provided their experimental data and derived volumetric kinetics for steam and CO_2 gasification of cylindrical char particles. Figure 4 depicts the mass loss of a cylindrical particle during CO_2 gasification at different temperatures T. As can be seen, the extended Layer Model can describe the increase of the gasifcation rate with increasing temperature and thus a faster conversion over time. At 1173 K the mass loss is slightly underpredicted, which can also be observed in [8] above 60 percent of conversion. The model predictions are in good accordance overall with the experimental results.

Figure 5 shows the simulation results of the extended Layer Model for steam gasification experiments of cylindrical particles with different diameters. As can be seen, the rise in the conversion time for increasing particle diameters d_p can be described by the Layer Model. The greatest deviations between model and measurements can be found for the intermediate particle size of d_p = 4.5 mm. However, very similar behavior is observed in [8] with a volumetric model, where their model notably underpredicts the mass loss for the same particle size. In general, the experiments at different particle sizes are satisfactorily described through the Layer Model.

In summary, with the novel model extension the Layer Model is able to suitably predict the gasification of biochar at different conditions. Despite the simplified formulation, a high quality of simu-

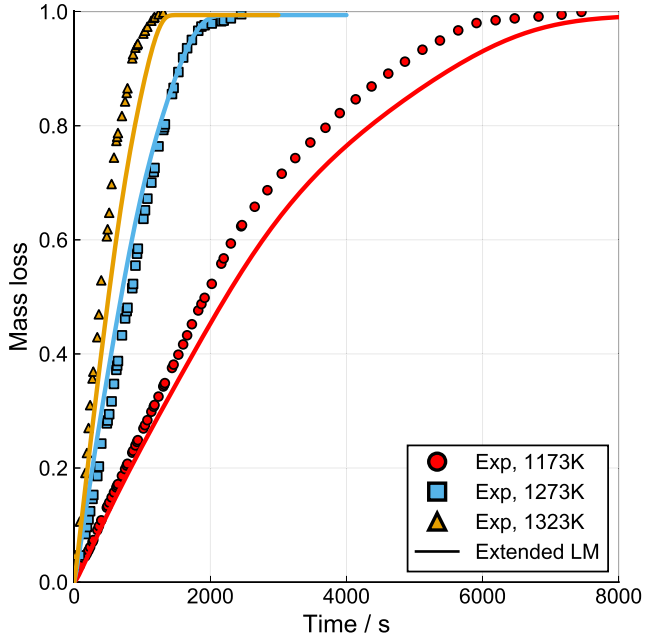

Fig. 4. Mass loss of a cylindrical char particle with $d_p = 5.5$ mm, $L_p = 10.5$ mm, $x_{CO_2} = 0.2$ and at varying bulk temperature T. Solid lines are extended Layer Model predictions, dots are experimental data from Van de steene et al. [8].

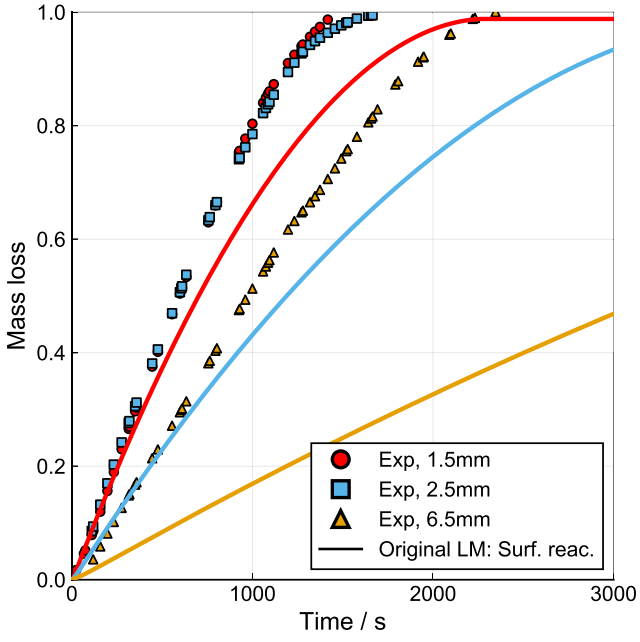

Fig. 6. Mass loss of a cylindrical char particle with $L_p = 10.5$ mm at $T = 1173$ K, $x_{H_2O} = 0.2$ and varying particle diameter d_p. Lines are original Layer Model predictions, dots are experimental data from Van de steene et al. [8].

lation results compared to the experimental data is achieved, similar to volumetric models reported in literature (e.g., [7,8]).

3.2. Model improvements

In the following section, the advantages of applying volumetric kinetics instead of the previously used surface kinetics at the reaction front shall be underlined. Subsequently, the model improvements provided by considering intraparticle diffusion shall be investigated.

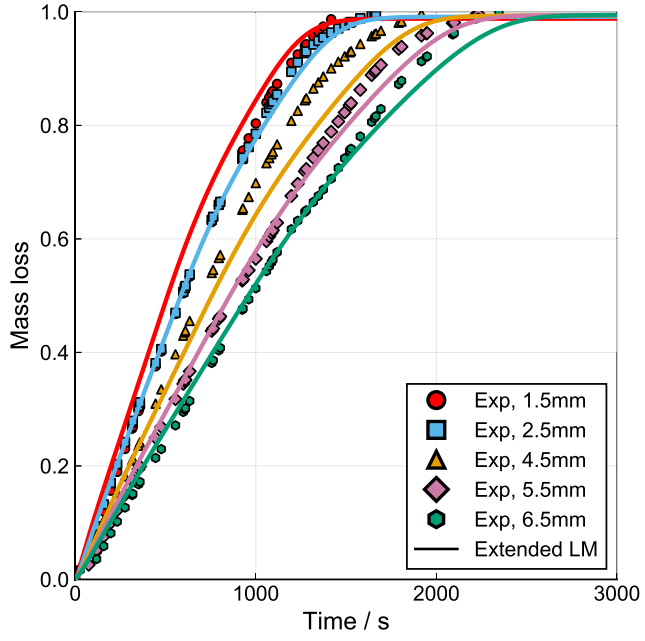

Fig. 5. Mass loss of a cylindrical char particle with $L_p = 10.5$ mm at $T = 1173$ K, $x_{H_2O} = 0.2$ and varying particle diameter d_p. Solid lines are extended Layer Model predictions, dots are experimental data from Van de steene et al. [8].

3.2.1. Volumetric vs. surface reactions

Despite their original design for lignite CO_2 gasification [16], Mehrabian et al. [3], Johansson et al. [17], Thunman et al. [9] and Gómez et al. [11] used the same (or similar) surface kinetics for CO_2 and/or steam gasification of biochar for their particle models. Thunman et al. also stated that gasification was not the focus for their publication. Since we focus mainly on gasification in this work, we intend to point out the possible problems of using surface kinetics from literature and applying them at a reaction front for biomass gasification. The steam gasification experiments of cylindrical char particles of varying thickness (i.e. diameter) by Van de steene et al. [8] from Section 3.1 shall be used for this reason.

The conversion rate for steam gasification originally implemented in the Layer Model (Eq. (6) and Table 1) is

$$-\dot{R}_C = 3.42 \cdot T_S \cdot \exp\left(\frac{-15\,600}{T_S}\right) A_S \cdot c_{A,S} \tag{20}$$

with A_S being the char layer surface area. Thus, the conversion rate is proportional to the external surface area at the reaction front ($\dot{R}_C \propto A_S$). Therefore, it is called a "surface reaction" in this work. For "volumetric reactions", the char conversion rate would be proportionate to the char layer volume V_C.

Figure 6 shows the simulation results versus the experimental data when applying this surface reaction scheme. In contrast to the volumetric reactions (Fig. 5), the surface reactions underpredict the char conversion rate for all particle sizes. Even though the simulations results are fairly reasonable for the smallest particle size (1.5 mm), the discrepancy increases significantly with a rising particle size. The model predicts a greater change in mass loss between the particle sizes than the measurements would suggest.

The volumetric kinetics by Van de steene et al. [8] were obviously derived from their experimental results and are expected to adequately describe their data. Therefore, it can also be expected that the original surface kinetics in Eq. (20) might not be able to perform equally well on the same set of data. However, the general problem lies not (only) in the kinetic parameters, but rather in the difference of scaling with particle size between surface kinetics and volumetric kinetics. In order to underline this issue, the

well-suited volumetric kinetics could be transformed into surface kinetics based on the Thiele modulus Φ.

When the Thiele modulus Φ is high (i.e. for big particles, fast reaction rates and/or slow intraparticle diffusion), intraparticle diffusion becomes the limiting process. Gaseous reactant A can no longer fully penetrate the particle, but is consumed close to the external particle surface instead. This model concept fits the idea of a surface reaction. In the limit of a high Thiele modulus Φ, the internal effectiveness factor η_{int} approaches $1/\Phi$ asymptotically [45]. Using Eq. (11) and Table 2, the actual reaction rate of char is then

$$-\dot{R}_{\text{C}}^{\text{act}} = -\eta_{\text{int}}(\Phi)\cdot V_{\text{C}}\cdot \dot{r}_{\text{C},S} \overset{(\Phi\gg 1)}{=\!=} \frac{1}{\Phi}\cdot V_{\text{C}}\cdot k_c\cdot c_{A,S}^{n}\cdot F(X). \tag{21}$$

Inserting Eq. (12) into Eq. (21) yields

$$-\dot{R}_{\text{C}}^{\text{act}} \overset{(\Phi\gg 1)}{=\!=} A_S\sqrt{\frac{2}{n+1}\cdot D_{\text{e},A}^{\text{C}}\cdot k_c\cdot c_{A,S}^{n+1}\cdot F(X)}. \tag{22}$$

Firstly, Eq. (22) shows that intraparticle-diffusion-limited reactions appear to have a different reaction order and activation energy than the original volumetric rate law would suggest. This is well-known and explained in detail in [28]. Secondly, the reaction rate in Eq. (22) is indeed proportional to the char layer surface area A_S instead of its volume V_{C}. Thus, when employing a volumetric rate law together with an effectiveness factor approach, strong diffusion limitation formally leads to a surface reaction.

With this in mind, an error estimation for employing a surface reaction rate instead of a volumetric reaction rate can be made. From Eq. (21) the ratio of the general reaction rate $\dot{R}_{\text{C}}^{\text{act}}$ and the intraparticle-diffusion-limited reaction rate $\dot{R}_{\text{C}}^{\text{act,diff}}$ is obtained.

$$\frac{\dot{R}_{\text{C}}^{\text{act}}}{\dot{R}_{\text{C}}^{\text{act,diff}}} = \frac{\eta_{\text{int}}(\Phi)}{1/\Phi} \tag{23}$$

In the denominator on the right-hand side of Eq. (23) a high Thiele modulus Φ is assumed, while the numerator holds for any Φ. Therefore, when the Thiele modulus Φ is small, the ratio will differ from one. This estimates the error introduced when assuming a surface reaction rate when instead a volumetric reaction rate would be needed. Reformulating Eq. (23) and inserting Eq. (14) yields

$$\delta_{\text{err}} = 1 - \frac{\dot{R}_{\text{C}}^{\text{act}}}{\dot{R}_{\text{C}}^{\text{act,diff}}} = 1 - \left(\frac{1}{\tanh(3\Phi)} - \frac{1}{3\Phi}\right) \tag{24}$$

for the estimated relative error δ_{err} between the two formulations. It is labeled estimated relative error, because the correlation $\eta(\Phi) = \eta_{\text{int}}(\Phi)$ for spherical particles is used. Figure 7 shows the estimated relative error δ_{err} and the effectiveness factor $\eta = \eta_{\text{int}}$ as functions of the Thiele modulus Φ. For $\Phi = 4$, which is often seen in the literature as the criterion for intraparticle diffusion limitation [28], the relative error is 0.083. For $\Phi < 4$, the error rapidly increases, since the approximation $\eta_{\text{int}} = 1/\Phi$ is not applicable at these conditions. Hence, the application of surface kinetics would lead to a large error. Figure 7 further gives the Φ-range of all cases considered in this work. As can be seen, volumetric kinetics are required for all of them due to high estimated relative errors δ_{err} otherwise.

It is worth mentioning that external mass transfer can also play an important role in char conversion processes. An example for relevant external mass transfer influence, indicated by mass transfer Biot numbers $Bi_{\text{M}} < 10$, is given in Section 3.2.2.

3.2.2. Intraparticle diffusion

Finally, the model improvement by considering intraparticle mass transfer limitations will be demonstrated. Mermoud et al. [7] presented experimental results for steam gasification of

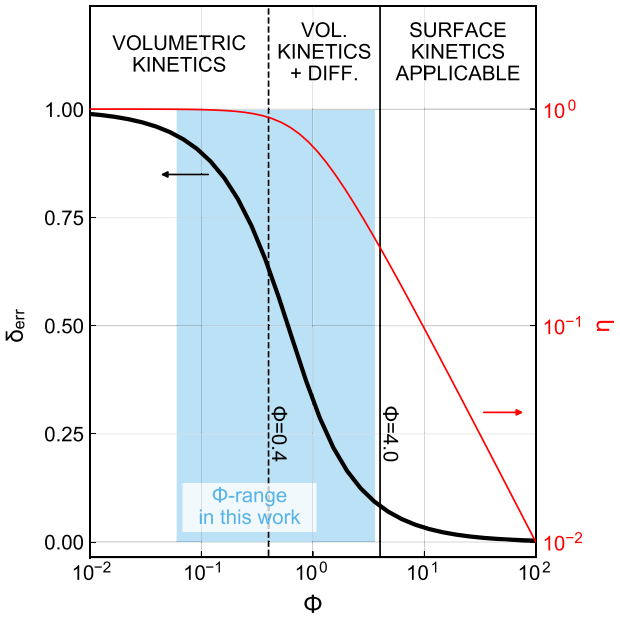

Fig. 7. Estimated relative error δ_{err} between actual volumetric and intraparticle-diffusion-limited reaction rates, internal effectiveness factor $\eta = \eta_{\text{int}}$ and range of Thiele moduli Φ for cases considered in this work.

bigger, spherical char particles alongside their volumetric rate law. Their reaction kinetics are given in Tables 2 and 4. Figure 8 shows the mass loss for particles with three diameters (10 mm, 20 mm and 30 mm) at two temperatures (1203 K and 1303 K, with only 10-mm-experimental-data available at 1303 K). There are two corresponding curves for every single one of these six cases. The dashed curve depicts the extended Layer Model result without intraparticle (pore) diffusion considered, i.e. $\eta = \eta_{\text{int}} = 1$. Conversely, the solid line depicts the extended Layer Model results considering intraparticle diffusion. For both temperatures, an increase in particle size leads to significant gaps between the two corresponding model curves. For the 10 mm and 20 mm particles, the Layer Model predictions with and without internal diffusion match the experimental data well. For $d_{\text{p}} = 30$ mm, the conversion rate is overpredicted significantly without intraparticle diffusion. The experimental mass loss is better described, especially towards the end, when considering internal diffusion. Even though measurements are only available for 10 mm at 1303 K, the simulations results for 20 mm and 30 mm are also given, just to underline the importance of internal diffusion modeling at elevated temperatures and bigger particle diameters.

Table 6 summarizes the calculated ranges of Thiele moduli Φ, internal effectiveness factors η_{int} and mass transfer Biot numbers Bi_{M} between the initial conversion state ($X = 0$) and nearly full conversion ($X = 0.99$). The effectiveness factors η_{int} decrease with increasing particle diameter d_{p} and temperature T, whereas the

Table 6
Thiele modulus Φ, internal effectiveness factor η_{int} and mass transfer Biot number Bi_{M} ranges between conversions $X = 0$ and $X = 0.99$ calculated for spherical particle cases. (*) Effective char diameters after pyrolysis are 7.05 mm, 14.07 mm, 20.87 mm, respectively.

T / K	d_{p} / mm	Φ	η_{int}	Bi_{M}
1203	10 (*)	0.27 – 0.56	0.85 – 0.96	1.72 – 2.16
	20 (*)	0.60 – 1.15	0.62 – 0.84	1.91 – 2.54
	30 (*)	0.95 – 1.80	0.45 – 0.69	2.05 – 2.82
1303	10 (*)	0.45 – 0.90	0.71 – 0.90	1.70 – 2.11
	20 (*)	1.03 – 2.10	0.40 – 0.66	1.88 – 2.47
	30 (*)	1.68 – 3.42	0.26 – 0.48	2.01 – 2.73

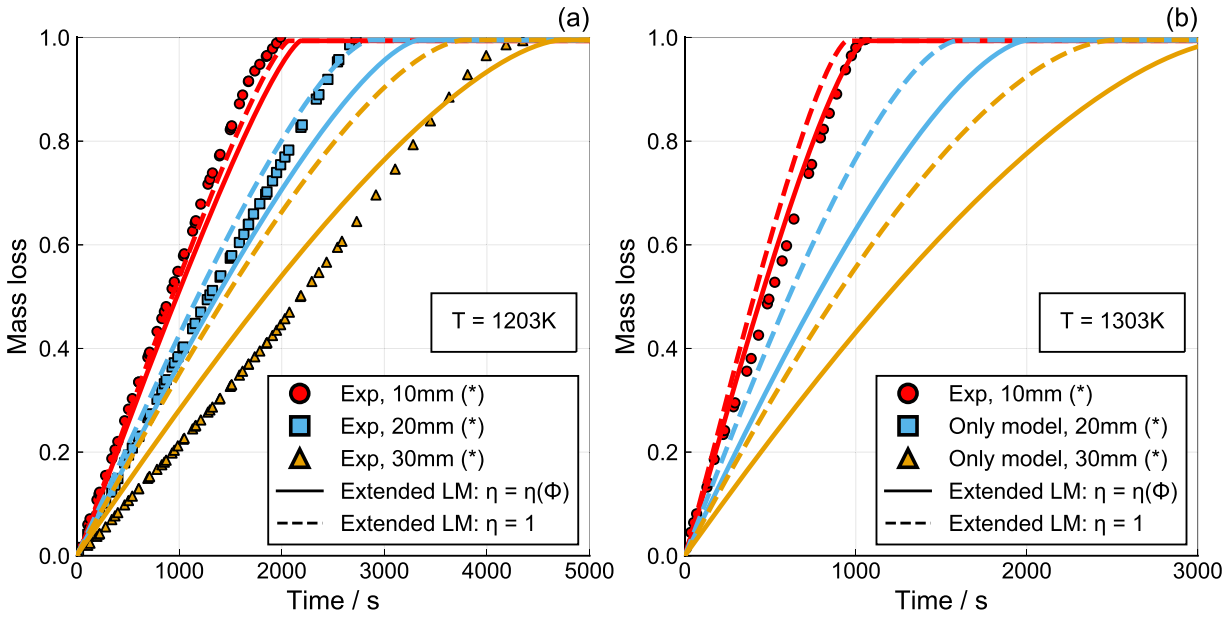

Fig. 8. Mass loss of a spherical char particle at $x_{H_2O} = 0.2$, varying particle diameter d_p and $T = 1203$ K (a) or $T = 1303$ K (b). Solid and dashed lines are extended Layer Model predictions (with and without intraparticle diffusion, respectively), dots are experimental data from Mermoud et al. [7]. (*) Effective char diameters after pyrolysis are 7.05 mm, 14.07 mm, 20.87 mm, respectively.

mass transfer Biot numbers Bi_M increase with increasing particle diameter d_p. Also, the dependency of the mass transfer Biot numbers Bi_M on the temperature T is relatively weak. Effectiveness factors η_{int} close to 1 for the smaller particles lead to a weak impact of intraparticle diffusion. However, for increasing particle size the effectiveness factors η_{int} drop significantly. Conversely, the increase of mass transfer Biot numbers Bi_M with particle size signifies enhanced external mass transfer. As can be seen from the range of mass transfer Biot numbers Bi_M, external mass transfer plays an important role for all the cases in Table 6.

3.3. Discussion

The extended Layer Model is validated for char gasification in Section 3.1, employing theoretical calculations and experimental data from literature. It is shown that the original Layer Model by Mehrabian et al. [3] is not able to properly describe the mass loss for the char gasification experiments by Van de steene et al. [8]. This is not only due to the different kinetic parameters used in the original model, but also due to the mathematical form of the surface kinetics employed at the layer boundary for the gasification reactions. It has been reported that the char reactivity depends on multiple parameters [2,18,20], which manifests itself in the great variety of kinetic data for char conversion in the literature. The kinetics parameters of the original surface reaction can be adjusted to give good results for one gasification experiment. However, the model is then still unable to predict the mass loss for the other experiments. For further details the reader is referred to the Supplementary Material provided together with this work.

The introduction of volumetric rate laws for char gasification solves this problem while maintaining the comparably simple model formulation of the Layer Model. Thus, low computational effort and good model predictions can be achieved, as showcased in Section 3.1. This extended Layer Model is flexible in terms of the volumetric rate law applied and allows for modeling of char conversion reactions throughout the entirety of the char layer, as opposed to interface-based reactions only.

Figure 7 can be used to estimate when it is viable to choose a simpler surface reaction model instead of a volumetric reaction model. If the Thiele modulus Φ is sufficiently high, the relative error between the volumetric formulation and the surface formulation becomes negligible. As can be seen, a volumetric reaction model is essential for all the cases considered in this work. The highest Thiele modulus $\Phi = 3.42$ is achieved with the biggest (20.87 mm) particles given by Mermoud et al. [7]. Even then, the relative error is still above 0.097. However, a surface reaction model would soon become viable for even larger particles, at higher temperatures and/or higher gas concentrations. Another feature of Fig. 7 is estimating the necessity of applying an effectiveness factor approach for volumetric rate laws. For example, with the smallest particles in this work, namely the 1.5 mm particles given by Van de steene et al. [8], the Thiele modulus Φ reaches values as low as 0.02. Under these conditions, the effectiveness factor $\eta = \eta_{int}$ is very close to 1, meaning that it will not influence the result significantly. As shown in Fig. 8, especially for bigger particles, intraparticle diffusion cannot be simply neglected.

The concept of Fig. 7 can be applied together with actual kinetics to estimate the model requirements under different experimental conditions. In Fig. 9, three regions are given based on temperature T and characteristic particle size Λ for the steam gasification kinetics by (a) Van de steene et al. [8] and (b) Mermoud et al. [7], respectively. For Thiele moduli $\Phi \leq 0.4$, meaning small particles and/or low temperatures, volumetric kinetics should be applied and intraparticle diffusion can be neglected (i.e. $\eta_{int} \approx 1$). For Thiele moduli $\Phi \geq 4.0$, meaning big particles and/or high temperatures, surface kinetics can be applied instead. Of course, volumetric kinetics together with an intraparticle diffusion model can also (always) be used. In the intermediate region, meaning $0.4 \leq \Phi \leq 4.0$, volumetric kinetics and an intraparticle diffusion model are required. As can be seen from the experimental data points in both Figures, the cases reported in this work are mostly in this intermediate region. Intraparticle diffusion can only be neglected for the smallest particles. Surface kinetics cannot be reliably applied for any of the cases. An additional feature when comparing Fig. 9 (a) and (b) is the fact that the limiting lines for $\Phi = 0.4$ and $\Phi = 4.0$ are not identical. This is because the kinetics of Van de steene et al. [8] and Mermoud et al. [7] are different, leading to different Thiele moduli Φ at a given temperature T and particle size

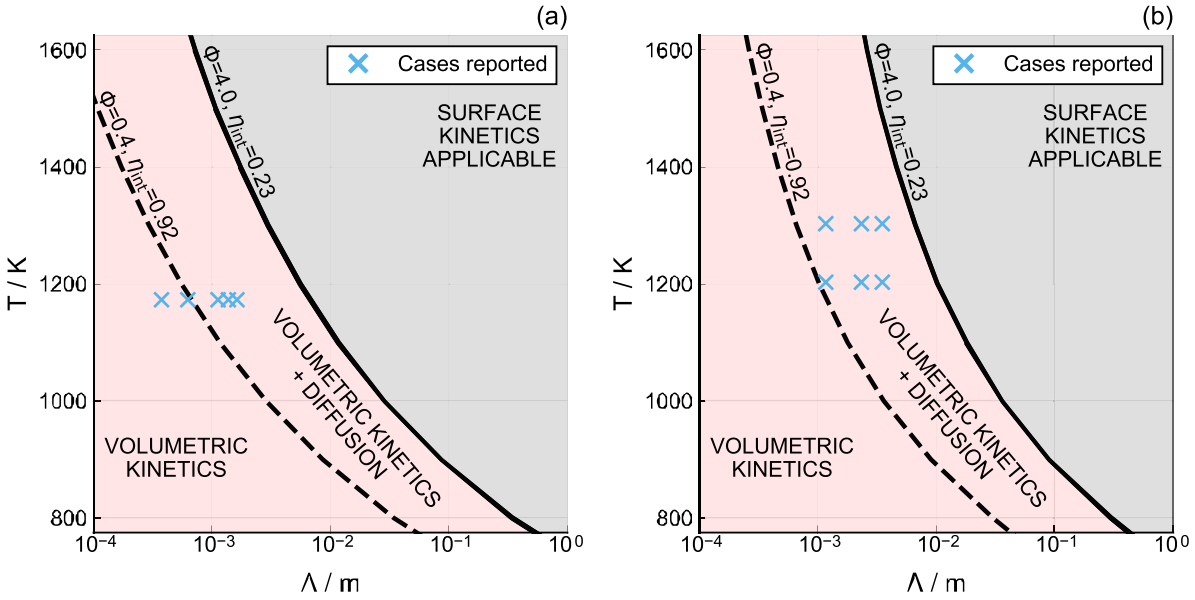

Fig. 9. Kinetic model requirements at different temperatures T and characteristic particle lengths Λ for experimental cases and kinetics reported by Van de steene et al. (a) or Mermoud et al. (b). Lines are calculated for respective steam gasification kinetics at $p_{H_2O} = 0.2$ atm and $X = 0.5$.

Λ. With this in mind, Fig. 9 can be used for first estimations under typical gasification conditions, but the specific model requirements depend on the kinetic model itself. It is also worth noting that the Thiele modulus Φ greatly depends on the effective diffusion coefficient $D^C_{e,A}$ and, thus, on the char porosity ε_C and possibly Knudsen diffusion limitations.

Finally, some model limitations should be addressed. They arise from the calculation of the effectiveness factor using correlations $\eta(\Phi) = \eta_{int}(\Phi)$ from the isothermal case. Since the effectiveness factor η takes values between 0 and 1 for the correlations reported in this work [28,35,36], it can never be greater than 1 (e.g. during exothermic reactions). Even though the heat of reaction is considered in this work, there is still only a single, isothermal char layer. Weisz and Hicks [46] have provided the fundamental concepts to tackle non-isothermal problems. Unfortunately, taking a non-isothermal char layer into consideration leads to much more complicated mathematical problems. In their recent publication, Bösenhofer and Harasek [47] address the drawback of isothermal effectiveness factor formulations within the scope of char conversion. However, since the char layer is treated as one isothermal volume in the Layer Model, no additional simplifications are needed in order to apply the isothermal effectiveness factor. The classic effectiveness factor formulation seems to be an appropriate, simple and fast solution.

Regarding the particle geometry, the char layer is typically a hollow volume (e.g. hollow sphere or hollow cylinder), because the wet and dry fuel layers are located at the center of the particle. Strictly speaking, the $\eta(\Phi) = \eta_{int}(\Phi)$ correlations discussed in this work were derived for full, solid volumes. If this effect needs to be considered, when dealing with drying, pyrolysis and fast char conversion in parallel, for example Burghardt and Kubaczka [48] present a suitable correlation. For char gasification at typical temperatures, since drying and pyrolysis are much faster, it can be neglected.

Despite the simplifications made in this work, the thermochemical conversion of biomass particles is still adequately described. The H_2O and CO_2 gasification reactions are endothermic and, as shown in Section 3.1, well predicted by the extended Layer Model. Furthermore, the layer model has already been successfully validated for pyrolysis and char oxidation in the literature [3,9–11,13]. In the case of char oxidation, an interface-based formulation seems more appropriate than for gasification due to typically high reaction rates and Thiele moduli Φ. However, for very slow oxidation processes, like smouldering, problems similar to those for gasification surface reactions could arise. Volumetric (i.e. mass-based) reaction rate formulations are already employed in the original Layer Model [3] for the pyrolysis reactions. As the devolatilization process is simply driven by temperature and not also by gaseous reactants, no additional efforts are made to describe pyrolysis reactions. If anything, the low temperature resolution of the Layer Model could prove to be a limiting factor in this regard. However, as shown in the aforementioned publications, the Layer Model can also achieve good predictions for pyrolysis.

4. Summary and conclusions

In this work, based on the model by Mehrabian et al. [3], an extension for the fast-solving Layer Model for single reactive biomass particles is presented. Char conversion was originally modeled using only surface reactions at the char layer boundary. While frequently applicable for biochar oxidation, biochar gasification has also commonly been modeled with similar surface reaction approaches in the literature. As shown in this work, these approaches cannot be employed reliably for typical char gasification kinetics at the temperature ranges (1173-1323 K) and the particle size ranges (1.5–20.87 mm) considered. The fundamental problems of these models are assessed and a solution in the form of volumetric reaction kinetics is presented. The model equations for applying volumetric rate laws are derived and a simple solution strategy is proposed. The model presented in this work is flexible in terms of possible rate laws and can be applied for different reaction orders. The effects of intraparticle diffusion are approximated using an effectiveness factor approach. It employs the well-known solution for first order reactions in spherical particles combined with appropriate scaling to account for differences in shape or kinetic formulations. Different rate laws or effectiveness factor equations can easily be implemented.

The extended Layer Model is first validated theoretically using the well-known analytical solution for first order reactions with external mass transfer from literature. It is further validated using the char gasification kinetics and experimental results by Van de steene et al. [8] as well as Mermoud et al. [7]. The model predic-

tions are in good accordance with the measured mass loss for the cases considered. Since the computationally fast, extended Layer Model now describes gasification satisfactorily, it can be used for particle-reactor coupling in holistic simulations of such processes in the future. Based on the data by Van de steene et al. it is shown that the original Layer Model is incapable of predicting the experimental results. The main reason for the deviations is the scaling of char conversion rates with external char layer surface as opposed to char layer volume. This is supported by the fact that adjusted kinetic parameters, which are able to describe one specific case, fail to describe the other cases (see also Supplementary Material).

Based on the Thiele modulus Φ, the general applicability of surface reactions versus volumetric reactions is discussed. For Thiele moduli $\Phi \geq 4$ both modeling approaches converge towards the same solution. Surface kinetics can thus be applied for large particles and/or high reaction rates. Furthermore, the importance of intraparticle diffusion is assessed. It can only be neglected when the Thiele modulus Φ is small (typically less than 0.4). This happens for small particles and/or at low temperatures.

Declaration of Competing Interest

The authors declare that they have no known competing financial interests or personal relationships that could have appeared to influence the work reported in this paper.

CRediT authorship contribution statement

Thomas Steiner: Conceptualization, Data curation, Investigation, Methodology, Software, Validation, Visualization, Writing – original draft. **Kai Schulze:** Conceptualization, Project administration, Supervision, Writing – review & editing. **Robert Scharler:** Funding acquisition, Supervision, Writing – review & editing. **Andrés Anca-Couce:** Conceptualization, Data curation, Investigation, Methodology, Software, Validation, Visualization, Writing – original draft.

Acknowledgments

The COMET Module BIO-LOOP (Austrian Research Promotion Agency Project Number 872189) is funded within COMET - Competence Centers for Excellent Technologies - by the Federal Ministry for Climate Action, Environment, Energy, Mobility, Innovation and Technology and the Federal Ministry for Digital and Economic Affairs as well as the co-financing federal province Styria. The COMET programme is managed by FFG (Austrian Research Promotion Agency, www.ffg.at/comet). The funding is gratefully acknowledged.

Supplementary material

Supplementary material associated with this article can be found, in the online version, at doi:10.1016/j.combustflame.2023.112940.

References

[1] M. Kaltschmitt, H. Hartmann, H. Hofbauer, Energie aus biomasse, 3rd ed., Springer, Berlin, Heidelberg, 2016.
[2] I. Haberle, Ø. Skreiberg, J. Łazar, N.E.L. Haugen, Numerical models for thermochemical degradation of thermally thick woody biomass, and their application in domestic wood heating appliances and grate furnaces, Prog. Energy Combust. Sci. 63 (2017) 204–252, doi:10.1016/j.pecs.2017.07.004.
[3] R. Mehrabian, S. Zahirovic, R. Scharler, I. Obernberger, S. Kleditzsch, S. Wirtz, V. Scherer, H. Lu, L.L. Baxter, A CFD model for thermal conversion of thermally thick biomass particles, Fuel Process. Technol. 95 (2012) 96–108, doi:10.1016/j.fuproc.2011.11.021.
[4] H. Lu, Experimental and modelling investigation of biomass particle combustion, Brigham Young University, 2006 Ph.D. thesis.
[5] A. Anca-Couce, N. Zobel, Numerical analysis of a biomass pyrolysis particle model: solution method optimized for the coupling to reactor models, Fuel 97 (2012) 80–88, doi:10.1016/j.fuel.2012.02.033.
[6] J.C. Wurzenberger, S. Wallner, H. Raupenstrauch, J.G. Khinast, Thermal conversion of biomass: comprehensive reactor and particle modeling, AIChE J. 48 (10) (2002) 2398–2411, doi:10.1002/aic.690481029.
[7] F. Mermoud, F. Golfier, S. Salvador, L. Van de Steene, J. Dirion, Experimental and numerical study of steam gasification of a single charcoal particle, Combust. Flame 145 (1) (2006) 59–79, doi:10.1016/j.combustflame.2005.12.004.
[8] L. Van de steene, J.P. Tagutchou, F.J. Escudero Sanz, S. Salvador, Gasification of woodchip particles: experimental and numerical study of char–H2O, char–CO2, and char–O2 reactions, Chem. Eng. Sci. 66 (2011) 4499–4509, doi:10.1016/j.ces.2011.05.045.
[9] H. Thunman, B. Leckner, F. Niklasson, F. Johnsson, Combustion of wood particles - a particle model for Eulerian calculations, Combust. Flame 129 (1) (2002) 30–46, doi:10.1016/S0010-2180(01)00371-6.
[10] H. Ström, H. Thunman, CFD simulations of biofuel bed conversion: a submodel for the drying and devolatilization of thermally thick wood particles, Combust. Flame 160 (2) (2013) 417–431, doi:10.1016/j.combustflame.2012.10.005.
[11] M. Gómez, J. Porteiro, D. Patiño, J. Míguez, Fast-solving thermally thick model of biomass particles embedded in a CFD code for the simulation of fixed-bed burners, Energy Convers. Manage. 105 (2015) 30–44, doi:10.1016/j.enconman.2015.07.059.
[12] R. Mehrabian, A. Shiehnejadhesar, R. Scharler, I. Obernberger, Multi-physics modelling of packed bed biomass combustion, Fuel 122 (2014) 164–178, doi:10.1016/j.fuel.2014.01.027.
[13] H. Ström, H. Thunman, A computationally efficient particle submodel for CFD-simulations of fixed-bed conversion, Appl. Energy 112 (2013) 808–817, doi:10.1016/j.apenergy.2012.12.057.
[14] T. Li, H. Thunman, H. Ström, A fast-solving particle model for thermochemical conversion of biomass, Combust. Flame 213 (2020) 117–131, doi:10.1016/j.combustflame.2019.11.018.
[15] F. He, F. Behrendt, A new method for simulating the combustion of a large biomass particle - a combination of a volume reaction model and front reaction approximation, Combust. Flame 158 (12) (2011) 2500–2511, doi:10.1016/j.combustflame.2011.04.016.
[16] M.L. Hobbs, P.T. Radulovic, L.D. Smoot, Modeling fixed-bed coal gasifiers, AIChE J. 38 (5) (1992) 681–702, doi:10.1002/aic.690380506.
[17] R. Johansson, H. Thunman, B. Leckner, Influence of intraparticle gradients in modeling of fixed bed combustion, Combust. Flame 149 (1) (2007) 49–62, doi:10.1016/j.combustflame.2006.12.009.
[18] C. Di Blasi, Combustion and gasification rates of lignocellulosic chars, Prog. Energy Combust. Sci. 35 (2) (2009) 121–140, doi:10.1016/j.pecs.2008.08.001.
[19] A. Anca-Couce, C. Hochenauer, R. Scharler, Bioenergy technologies, uses, market and future trends with Austria as a case study, Renew. Sustain. Energy Rev. 135 (2021) 110237, doi:10.1016/j.rser.2020.110237.
[20] A. Gómez-Barea, B. Leckner, Modeling of biomass gasification in fluidized bed, Prog. Energy Combust. Sci. 36 (4) (2010) 444–509, doi:10.1016/j.pecs.2009.12.002.
[21] G. Archan, A. Anca-Couce, J. Gregorc, M. Buchmayr, C. Hochenauer, J. Gruber, R. Scharler, Detailed experimental investigation of the spatially distributed gas release and bed temperatures in fixed-bed biomass combustion with low oxygen concentration, Biomass Bioenergy 141 (2020) 105725, doi:10.1016/j.biombioe.2020.105725.
[22] J. Adánez, A. Abad, F. García-Labiano, P. Gayán, L.F. de Diego, Progress in chemical-looping combustion and reforming technologies, Prog. Energy Combust. Sci. 38 (2) (2012) 215–282, doi:10.1016/j.pecs.2011.09.001.
[23] J. Adánez, A. Abad, T. Mendiara, P. Gayán, L. de Diego, F. García-Labiano, Chemical looping combustion of solid fuels, Prog. Energy Combust. Sci. 65 (2018) 6–66, doi:10.1016/j.pecs.2017.07.005.
[24] H. Ge, W. Guo, L. Shen, T. Song, J. Xiao, Biomass gasification using chemical looping in a 25kWth reactor with natural hematite as oxygen carrier, Chem. Eng. J. 286 (2016) 174–183, doi:10.1016/j.cej.2015.10.092.
[25] B. Dou, H. Zhang, Y. Song, L. Zhao, B. Jiang, M. He, C. Ruan, H. Chen, Y. Xu, Hydrogen production from the thermochemical conversion of biomass: issues and challenges, Sustain. Energy Fuels 3 (2019) 314–342, doi:10.1039/C8SE00535D.
[26] R. Taylor, R. Krishna, Multicomponent mass transfer, John Wiley & Sons, 1993.
[27] C. Wen, Noncatalytic heterogeneous solid-fluid reaction models, Ind. Eng. Chem. 60 (9) (1968) 34–54, doi:10.1021/ie50705a007.
[28] O. Levenspiel, Chemical reaction engineering, 3rd ed., John Wiley & Sons, 1999.
[29] A. Gómez-Barea, P. Ollero, R. Arjona, Reaction-diffusion model of TGA gasification experiments for estimating diffusional effects, Fuel 84 (12) (2005) 1695–1704, doi:10.1016/j.fuel.2005.02.003.
[30] A. Gómez-Barea, P. Ollero, An approximate method for solving gas–solid non-catalytic reactions, Chem. Eng. Sci. 61 (11) (2006) 3725–3735, doi:10.1016/j.ces.2005.12.023.
[31] A. Gómez-Barea, P. Ollero, C. Fernández-Baco, Diffusional effects in CO2 gasification experiments with single biomass char particles. 1. Experimental investigation, Energy Fuels 20 (5) (2006) 2202–2210, doi:10.1021/ef050365a.
[32] A. Gómez-Barea, P. Ollero, A. Villanueva, Diffusional effects in CO2 gasification experiments with single biomass char particles. 2. Theoretical predictions, Energy Fuels 20 (5) (2006) 2211–2222, doi:10.1021/ef0503663.
[33] R. Aris, On shape factors for irregular particles - I: the steady state problem. diffusion and reaction, Chem. Eng. Sci. 6 (6) (1957) 262–268, doi:10.1016/0009-2509(57)85028-3.

[34] J. Gottifredi, E. Gonzo, O. Quiroga, Isothermal effectiveness factor - I: analytical expression for single reaction with arbitrary kinetics. Slab geometry, Chem. Eng. Sci. 36 (4) (1981) 713–719, doi:10.1016/0009-2509(81)85086-5.
[35] J. Gottifredi, E. Gonzo, O. Quiroga, Isothermal effectiveness factor - II: analytical expression for single reaction with arbitrary kinetics, geometry and activity distribution, Chem. Eng. Sci. 36 (4) (1981) 721–730, doi:10.1016/0009-2509(81)85087-7.
[36] S. Cloete, A. Giuffrida, M. Romano, P. Chiesa, M. Pishahang, Y. Larring, Integration of chemical looping oxygen production and chemical looping combustion in integrated gasification combined cycles, Fuel 220 (2018) 725–743, doi:10.1016/j.fuel.2018.02.048.
[37] E.W. Thiele, Relation between catalytic activity and size of particle, Ind. Eng. Chem. 31 (7) (1939) 916–920, doi:10.1021/ie50355a027.
[38] G.F. Froment, K.B. Bischoff, Chemical reactor design and analysis, 1st ed., John Wiley & Sons, 1979.
[39] J. Szekely, J.W. Evans, H.Y. Sohn, Gas-solid reactions, Academic Press, Inc., 1976.
[40] S. Noorman, F. Gallucci, M. van Sint Annaland, J. Kuipers, A theoretical investigation of CLC in packed beds. Part 1: particle model, Chem. Eng. J. 167 (1) (2011) 297–307, doi:10.1016/j.cej.2010.12.068.
[41] R.B. Bird, W.E. Stewart, E.N. Lightfoot, Transport phenomena, 2nd ed., John Wiley & Sons, 2002.
[42] S.W. Churchill, M. Bernstein, A correlating equation for forced convection from gases and liquids to a circular cylinder in crossflow, J. Heat Transf. 99 (2) (1977) 300–306, doi:10.1115/1.3450685.
[43] VDI-Gesellschaft Verfahrenstechnik und Chemieingenieurwesen, VDI Heat atlas, 2nd ed., Springer, Berlin, Heidelberg, 2010.
[44] J.R. Cash, A.H. Karp, A variable order Runge-Kutta method for initial value problems with rapidly varying right-hand sides, ACM Trans. Math. Softw. 16 (3) (1990), doi:10.1145/79505.79507.
[45] K.B. Bischoff, Effectiveness factors for general reaction rate forms, AIChE J. 11 (2) (1965) 351–355, doi:10.1002/aic.690110229.
[46] P. Weisz, J. Hicks, The behaviour of porous catalyst particles in view of internal mass and heat diffusion effects, Chem. Eng. Sci. 17 (4) (1962) 265–275, doi:10.1016/0009-2509(62)85005-2.
[47] M. Bösenhofer, M. Harasek, Non-isothermal effectiveness factors in thermochemical char conversion, Carbon Resour. Convers. 4 (2021) 47–54, doi:10.1016/j.crcon.2021.01.004.
[48] A. Burghardt, A. Kubaczka, Generalization of the effectiveness factor for any shape of a catalyst pellet, Chem. Eng. Process. 35 (1) (1996) 65–74, doi:10.1016/0255-2701(95)04115-X.